



AIAA 2002-5115

**Prediction of Drag Reduction in Supersonic
and Hypersonic Flows with Counterflow Jets**

**Endwell O. Daso
Boeing Phantom Works
Long Beach, California**

**Warren Beaulieu
Boeing Phantom Works
Long Beach, California**

**James O. Hager
Boeing Phantom Works
Long Beach, California**

**AIAA/AAAF 11th International Space Planes
and Hypersonic Systems and Technologies
Conference**

29 September – 04 October, 2002 / Orleans, France



Prediction of Drag Reduction in Supersonic and Hypersonic Flows with Counterflow Jets

Endwell O. Daso*[◆]
Boeing Phantom Works
Long Beach, CA 90807

Warren Beaulieu*
Boeing Phantom Works
Long Beach, CA 90807

and

James O. Hager[☐]
Boeing Phantom Works
Long Beach, CA 90807

Abstract

Computational fluid dynamics solutions of the flowfield of a truncated cone-cylinder with and without counterflow jets have been obtained for the short penetration mode (SPM) and long penetration mode (LPM) of the freestream-counterflow jet interaction flowfield. For the case without the counterflow jet, the comparison of the normalized surface pressures showed very good agreement with experimental data. For the case with the SPM jet, the predicted surface pressures did not compare as well with the experimental data upstream of the expansion corner, while aft of the expansion corner, the comparison of the solution and the data is seen to give much better agreement. The difference in the prediction and the data could be due to the transient character of the jet penetration modes, possible effects of the plasma physics that are not accounted for here, or even the less likely effect of flow turbulence, etc. For the LPM jet computations, one-dimensional isentropic relations were used to derive the jet exit conditions in order to obtain the LPM solutions. The solution for the jet exit Mach number of 3 shows a jet penetration several times longer than that of the SPM, and therefore much weaker bow shock, with an attendant reduction in wave drag. The LPM jet is, in essence, seen to be a "pencil" of fluid, with much higher dynamic pressure, embedded in the oncoming supersonic or hypersonic freestream. The methodology for determining the conditions for the LPM jet could enable a practical approach for the design and application of counterflow LPM jets for the reduction of wave drag and heat flux, thus significantly enhancing the aerodynamic characteristics and aerothermal performance of supersonic and hypersonic vehicles. The solutions show that the qualitative flow structure is very well captured. The obtained results, therefore, suggest that counterflowing jets are viable candidate technology concepts that can be employed to give significant reductions in wave drag, heat flux, and other attendant aerodynamic benefits.

Introduction

The efficiency and performance of any air vehicle is dictated by the physics of the flowfield of the vehicle and/or propulsion system. The flowfields of supersonic and hypersonic vehicles and propulsion systems are characterized by strong shock systems, which may include different types of shocks: oblique (forebody, inlet) shocks, normal shocks and other shock structures and interactions. For a given geometry, the strength of the shocks increases with increasing flow Mach number.

Strong shocks contribute disproportionately to the drag of the vehicle, and may cause severe aerothermal loads, which could translate into poor aerodynamic performance (lift/drag) and stringent thermal protection system requirements, i.e. severe penalties in vehicle range and weight, etc., for single- or two-stage transatmospheric cruise and reentry vehicles.

As an example, the interaction of the forebody nose shock with the engine cowl leading edge of a highly integrated supersonic or hypersonic vehicle, a Type IV interaction, can result in severe thermal loads that may cause structural degradation or failure. Similarly, the management of sonic boom, the reflection of the shock system of supersonic and hypersonic vehicles by the ground, has remained a technologically challenging problem in the design of environmentally compatible supersonic and hypersonic cruise vehicles.

* Product Engineering Project Specialist, Senior Member

◆ Presently Group Lead, NASA Marshall Space Flight Center, Marshall Space Flight Center, AL 35812

✱ Project Manager

☐ Senior Engineer

and disperse the strong shock system of supersonic and hypersonic flows in order to reduce wave drag, aerothermal loads, as well as attenuate sonic boom, etc. That is, the creation of a flowfield about the vehicle, in which the shock system is rendered very weak or almost "shockless," thereby significantly enhancing the vehicle aerodynamic efficiency and performance. The immediate impact of such flowfields is a significant improvement in the aerothermal characteristics of the vehicle surfaces, and vehicle cross-range authority, etc., particularly for transatmospheric cruise, and reentry vehicles, and other reusable launch systems.

Background

Concepts to enhance the aerodynamic and aerothermal performance of supersonic and hypersonic vehicles by weakening the shock system are not new [1-7]. Resler and Sears [2] explored the use of electromagnetic effects to improve aerodynamic performance, while Ziemer [4] demonstrated the effects of magnetic fields on the standoff distance of the bow shock of a sphere in a supersonic stream. Ziemer's results show the bow shock to be significantly diffused, with an attendant increase in the shock standoff distance due to the interaction of the magnetic field with the flow.

In recent years, there has been a strong and renewed interest in the application of weakly ionized nonequilibrium plasmas (WINPs) or cold plasmas, which by definition has a very low degree of ionization, $O(10^{-8}$ to $10^{-5})$, as a candidate concept for the reduction of wave drag and heat flux of bodies in supersonic and hypersonic flows. Experiments in Russia and the United States [8-24] reveal that cold plasma introduced into high speed flows produce various anomalous effects. For supersonic flows over blunt bodies, the anomalous effects include an increase in the "speed of sound," shock acceleration, dispersion and attenuation, with attendant reductions in wave drag and heat flux.

The aerodynamic effects of WINPs in supersonic and hypersonic flows such as drag reduction are widely reported. *However, the flow physics is still not well understood*, which has prompted the ongoing debate whether the anomalous behavior is due to thermal effects or gradients (localized Joule heating, etc.) or nonequilibrium gasdynamic processes: ion acoustic waves, electron heat conduction, double layer (charge separation), streamer/shock interactions, etc., or the complementary effects of thermal gradients and nonequilibrium plasma physics. More recent work [24-31] make a stronger argument for the effects of thermal gradients to explain the anomalous flow behavior due to cold plasma, while Ref. 20 reports similar effects even

for Helium plasma generated in a shock tube near room temperature. Others [25,32,33] attribute it to nonequilibrium processes, such as vibrational relaxation to account for the drag reduction. We will not further discuss these different points of view since it is beyond the scope of the work here.

One candidate concept that has received considerable attention recently in the application of cold plasma for wave drag reduction is counterflow jets. The effects of counterflow jets for the reduction of wave drag in high speed flows have been investigated by several authors [1,5-7,22-24]. Shang [24] investigated both experimentally and computationally the aerodynamic effects of various counterflow jets, both with and without plasma, to determine the amount of drag reduction in a hypersonic flow over a sphere. The jet penetration was observed to have two stability modes, an unsteady oscillatory motion under a subcritical state and nearly steady supercritical state beyond the shock bifurcation point, depending on the driving stagnation pressure and mass flow rate of the jet. The drag reduction was observed to strongly depend on the jet mass flow rate. For the jet without plasma, the trend was computationally and experimentally observed to be the same for the counterflow jet with plasma, though the plasma jet gave about 10% higher reduction in drag, compared to that at room temperature, which is attributed to the deposited plasma thermal energy.

Formin, et. al. [23] investigated different jet penetrations in counterflow plasma jet or "aerospike" experiments. In these tests, plasma jets from truncated cone-cylinder models, with surface pressure taps for surface pressure data, were injected into oncoming supersonic freestreams at Mach numbers of 2, 2.5 and 4. The plasma generator is instrumented inside the cone-cylinder model. These experiments reveal that there are two modes of jet penetration, a short penetration mode (SPM) and a long penetration mode (LPM), which are coupled through transitional modes of the jet-freestream interactions. The SPM and LPM were determined by correlation to the pressure ratio of the jet stagnation pressure to that of the total pressure behind the normal shock. It was observed that the jet interaction mode typically started out in the LPM and transitioned to the SPM, depending on the pressure ratio. The SPM was observed when the pressure ratio was found to be less than 2, and the LPM resulted in significantly higher reduction in drag, with an attendant effect of weakening the bow shock.

Formin, et. al. [23] also carried out an inviscid computational fluid dynamic (CFD) analysis to predict both the SPM and LPM modes and compared their

solutions with the experimental data. The comparisons were reported to show good agreement. However, to predict the LPM, the counterflow jet stagnation pressure (or pressure ratio) was arbitrarily varied until the desired flow structure was obtained. It is, therefore, not clear that a single flow variable or parameter such as the pressure ratio is the only mode discriminator or the appropriate scaling parameter to determine the SPM and LPM interactions.

In the analysis that follows, we will employ a more methodological approach, based on one-dimensional isentropic relations, to establish the jet flow conditions that yield the LPM to define a practical approach to enable the design and application of the counterflow jet concept for wave drag and heat flux reduction. The goal here is therefore to numerically predict the flow physics of the LPM mode as a result of the interaction of the counterflowing jets with the oncoming freestream, to accurately assess the benefits of the LPM in terms of significant increases in wave drag reduction. This could also benefit efforts to mitigate sonic boom [34], since sonic boom is the manifestation of the reflection of the shock system of high-speed vehicles by the ground, a much weaker shock system will also give a more environmentally tolerable lower “boom.”

Analysis

The flowfield of the classical de Laval nozzle in an ambient environment is dictated by the expansion of the nozzle flow, i.e., whether the nozzle is underexpanded, fully expanded or overexpanded. For fully expanded nozzle flows, that is, the static pressure at the nozzle exit is the same as the ambient pressure of the surrounding freestream, the solution of the flowfield can be obtained analytically, for example, by the classical method of characteristics (MOC). Therefore, for co-flowing nozzle flows, the conditions at the boundary defined by the exit of the nozzle relative to the freestream may be known a priori, and the corresponding flow structure is thus easily obtained from analytical or numerical solutions, since the problem is mathematical well posed to give unique solutions. Indeed, if the flow is everywhere supersonic, the solution can be obtained in a piecemeal approach, that is the conditions of the nozzle exit plane can be used as the inflow boundary condition for the solution of the flowfield of the supersonic jet downstream for any given nozzle exit Mach number.

For nozzle flows issuing in a direction opposite to the freestream, that is, counterflowing jets, the mathematical simplicity is lost with respect to the boundary conditions at the exit of the nozzle, and the

resulting flow structure becomes extremely complicated, particularly for flows issuing from truncated surfaces, for which the resulting flow structures contain embedded subsonic and recirculating pockets, even away from solid surfaces. For this case, the amount of the reduction in the wave drag and heat flux, whether it is a cold, heated or plasma jet, strongly depends directly on the degree of penetration of the jet, that is, whether the jet is in the SPM or LPM, as shown by the analyses of Formin et. al. [23]. Therefore, in order to employ the counterflow jet as a practical technology concept for wave drag and heat flux management, it is critical to design systems that will operate optimally, that is, for the jets to give the LPM.

To derive the applicable equations for the prediction of the LPM, we assume that the stagnation conditions of the counterflow jet that gives a jet exit Mach number of 1 is known. Based on these assumption, we employ one-dimensional isentropic equations to obtain the relations that govern the expansion of the counterflow jet in order to obtain the LPM jet-shock interaction to give the desired reductions in wave drag.

We start out by stating the constraints between the flow rate at any other jet exit Mach number relative to that of the Mach 1 or reference exit flow. That is

$$\rho_2 u_2 A_2 = k \rho_1 u_1 A_1 , \quad (1)$$

where ρ_1 , u_1 , and A_1 are the density, streamwise jet velocity, and cross-sectional area of the counterflow jet nozzle exit Mach number of 1, respectively. Similarly, ρ_2 , u_2 , and A_2 are the corresponding values of the jet with exit Mach number greater than 1. In Eq. 1, k is simply a constant of proportionality between the two counterflow jet flow rates. For the same jet nozzle or injector, $A_1 = A_2$. Since our interest here is to establish the flow conditions at the exit of the counterflow jet to obtain the LPM, we assume that the geometry of the injector is the same for both SPM and LPM. This assumption is not restrictive. Thus, Eq. 1 becomes

$$\rho_2 u_2 = k \rho_1 u_1 . \quad (2)$$

Starting with the one-dimension isentropic equations, the stagnation conditions for the case in which the counterflow jet exit Mach number is supersonic relative to the jet with an exit Mach 1 can be shown to be

$$\frac{p_{02}}{p_{01}} = k^2 \frac{\rho_{02}}{\rho_{01}} \left[\frac{M_2}{M_1} \right]^2 \left[\frac{1 + \frac{\gamma-1}{2} M_2^2}{1 + \frac{\gamma-1}{2} M_1^2} \right]^{\frac{\gamma+1}{\gamma-1}} , \quad (3)$$

where p_{01} , ρ_{01} , M_1 are, respectively, the stagnation pressure, stagnation density and exit Mach number for the counterflow jet with an exit Mach number, $M_1 = 1$, while p_{02} , ρ_{02} , M_2 are the corresponding notations for the counterflow jet whose exit Mach number is greater than 1.

Assuming that the test gas of the counterflow jet is thermally and calorically perfect, then from the equation of state we obtain

$$\frac{T_{02}}{T_{01}} = \left[k \frac{\rho_{02} M_2}{\rho_{01} M_1} \right]^2 \left[\frac{1 + \frac{\gamma-1}{2} M_2^2}{1 + \frac{\gamma-1}{2} M_1^2} \right]^{\frac{\gamma+1}{\gamma-1}}, \quad (4)$$

where T_{01} , is the stagnation temperature for the counterflow jet with an exit Mach number of 1, and T_{02} is stagnation temperature for the counterflow jet whose exit Mach number is greater than 1. In Eqs. 3 and 4, γ is the ratio of specific heats, which is assumed to remain about the same at the two stagnation temperatures, which only holds if the difference in the temperatures are small. This is not generally the case. The error implicit in this assumption can readily be accounted for.

Equations 3 and 4 contain the ratio of the stagnation densities, ρ_{02}/ρ_{01} , which needs to be specified in other to determine p_{02}/p_{01} and T_{02}/T_{01} for a given k and M_1 . For simplicity, we imposed the constraint

$$\rho_{02} = \rho_{01}/k^2. \quad (5)$$

which allows one to determine p_{02}/p_{01} and T_{02}/T_{01} completely for a given k and M_1 .

Numerical Simulations

The application of Eqs. 3 through 5 in the simulation of counterflowing jets depends on the particular CFD code in terms of how the flowfield is normalized, initialized and/or how the freestream and counterflow jet conditions are specified. For this analysis, the CFD code we employed is the CFL3D [35], Version 6.0. In CFL3D, the velocity field is normalized by the freestream speed of sound, a_∞ , density by ρ_∞ and the pressure and energy by \mathcal{P}_∞ . Note that the freestream values denoted by the subscript ∞ here corresponds to the freestream values denoted by superscript \sim and the subscript ∞ in Ref. 35. Therefore, using Eqs. 3 and 4,

we derive the corresponding expressions for the normalized boundary conditions for the counterflow jet, that is, at the jet exit plane, if the solution for the jet starts from the jet exit.

The equation for the nondimensionalized velocity, pressure and density are, respectively, given by

$$\frac{u_2}{a_\infty} = M_2 \left(\frac{T_{01} T_{02}}{T_{0\infty} T_{01}} \left[\frac{1 + \frac{\gamma-1}{2} M_\infty^2}{1 + \frac{\gamma-1}{2} M_2^2} \right] \right)^{\frac{1}{2}}, \quad (6)$$

$$\frac{p_2}{\mathcal{P}_\infty} = \frac{1}{\gamma} \frac{p_{01} p_{02}}{p_{0\infty} p_{01}} \left[\frac{1 + \frac{\gamma-1}{2} M_\infty^2}{1 + \frac{\gamma-1}{2} M_2^2} \right]^{\frac{\gamma}{\gamma-1}}, \quad (7)$$

and

$$\frac{\rho_2}{\rho_\infty} = \frac{\rho_{01} \rho_{02}}{\rho_{0\infty} \rho_{01}} \left[\frac{1 + \frac{\gamma-1}{2} M_\infty^2}{1 + \frac{\gamma-1}{2} M_2^2} \right]^{\frac{1}{\gamma-1}}. \quad (8)$$

Lastly, the ratio of the dynamic pressures of the counterflow jets with exit Mach numbers of M_1 and M_2 can be shown to be

$$\frac{q_2}{q_1} = k \frac{u_2}{u_1}. \quad (9)$$

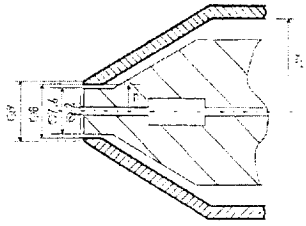
If the computations for the counterflow jet is started from the jet reservoir or stagnation chamber, then Eqs. 3, 4 and 5 must be used directly, or used to determine the normalized flowfield variables at the jet exit, depending on the CFD code in question.

In terms of the description of the CFD code, CFL3D is a three-dimensional, time-accurate, finite-volume, compressible thin layer Navier-Stokes (TLNS) code, which can also be run in inviscid (Euler) mode. It has a suite of turbulence models: zero-equation and various one-equation and two-equation turbulence models for turbulent flowfield computations, as well as van Leer's flux-vector and Roe's flux-difference splitting algorithms to compute fluxes. It also has multi-block, grid sequencing and multi-gridding capabilities to enhance solution convergence rates. The code is very well documented and is publicly available. As such, we will not give detailed description of the code here. The

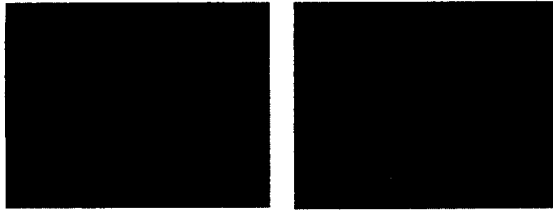
interested reader is, therefore, referred to the CFL3D User's Manual [35] for further details of the code.

Flowfield Computation of the SPM and LPM

As a test problem, we consider the flowfield of a counterflowing jet in an oncoming freestream. The geometry is one of the truncated cone-cylinder models of Refs. 22 and 23, as shown in Fig. 1.



a) Schematic of the geometry [22,23]



b) Without plasma nozzle

c) With plasma nozzle

Figure 1. Truncated cone-cylinder geometry [22,23].

The freestream Mach number, M_∞ , the stagnation pressure, $p_{0\infty}$ and stagnation temperature, $T_{0\infty}$ are, respectively, 2, 97.0kPa and 291.9K. For the counterflow jet, the exit Mach number, M_1 , the stagnation pressure, p_{01} and stagnation temperature, T_{01} are 1, 360.0kPa and 4840K, respectively. Further details of the geometry and the flow environments of the freestream and the counterflow jet stagnation conditions are given in Refs. 22 and 23. The counterflow jet stagnation and exit conditions for Mach numbers greater than 1 are obtained from Eqs. 3 through 8. In these computations, we assume $k = 1$, that is the flow rates of the counterflow jets with jet exit Mach

numbers of 1 and higher than 1 are the same. Table 1 shows the values of ρ_{02}/ρ_{01} , p_{02}/p_{01} , T_{02}/T_{01} , u_2/a_∞ , p_2/\mathcal{P}_∞ , ρ_2/ρ_∞ and q_2/q_1 for various values of counterflow jet exit Mach numbers, M_2 .

Computation Grid

The computational grid employed for the solution of the freestream-counterflow jet flowfield is a structured full three-dimensional C-H grid topology, and is made of three blocks, with dimensions of 17X189X57, 57X9X9 and 49X9X9 for the external flow, counterflow jet or core and the nozzle injector, respectively. Though the nozzle injector was gridded, the nozzle grid was not used in the computation. That is the counterflow jet flow was started from the exit or outflow plane of the nozzle injector. The grid was highly resolved near the wall and in the region of the counterflow jet to accurately capture the complex flow structure of the interactions. The upstream and outflow boundaries of the grid were extended far enough to adequately define the freestream and the counterflow jet domain. Figure 2 shows a quadrant of the three-dimensional grid.

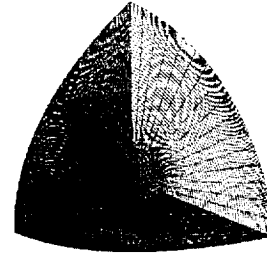


Figure 2. Computational grid of the cone-cylinder.

Results

Before we start to discuss the results of the analysis, we should point out that the computations for the counterflow jet do not take into account any effects of the ionized jet or plasma, as in the experiments of Formin, et. al. [23], since the TLNS equations in CFL3D do not have any plasma physics. As such these results only manifest the effects of the fluid dynamic interactions between the heated jet and the oncoming

M_2	ρ_{02}/ρ_{01}	p_{02}/p_{01}	T_{02}/T_{01}	u_2/a_∞	p_2/\mathcal{P}_∞	ρ_2/ρ_∞	q_2/q_1
2.0	1.0	2.847656	2.847656	13.7429324	7.5490151	0.2238306	2.7556670
3.0	1.0	17.931565	17.931565	41.4756524	10.1256192	0.0741661	8.3166526
4.0	1.0	114.891606	114.891606	114.2934583	15.6953956	0.0269140	22.9176514

Table 1. Computed stagnation and counterflow jet exit flow conditions for various jet exit Mach numbers for $k = 1$, $M_1 = 1$.

the external flow. Secondly, we also point out that the solutions presented are laminar steady state solutions.

We start with the comparison of the solutions of the flowfields with and without the counterflow jet, with an exit Mach number of 1, which is one of the test cases of Refs. 22 and 23. This is shown in Fig. 3.

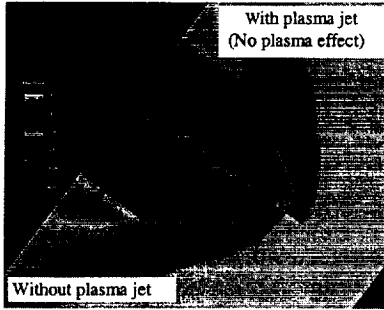


Figure 3. Mach number distributions.

The comparison shows the effects of the counterflow jet on the external freestream. One readily sees that the standoff distance of bow shock of the truncated conecylinder is increased by more that a factor of two, thus indicating a much weaker bow shock, with an attendant reduction in wave drag, which is in consistent with previous work [22,23,24]. Also clearly noticeable in the figure is the flow over the truncation and the conecylinder, which shows a larger subsonic region for the flow with jet. Lastly, the upstream penetration of the jet into the oncoming external freestream is about the same scale of the diameter of the truncated face. This mode of penetration is the short penetration mode (SPM).

To get a better understanding of the differences in the flow structure of the two flowfields, Fig. 4 shows the velocity vectors in the vicinity of the face of the truncation. The color indicates velocity magnitude. The figure shows multiple vortex structures, one on the wall of the truncated face, while the others are embedded in the flow as the jet rapidly decelerates after



Figure 4. Velocity vectors

reaching the peak velocity through the expansion, as it interacts with the external oncoming freestream. Qualitatively, the solution of Fig. 4 is very consistent with the schematic of the flow structure of Ref. 23, Fig.5, for the SPM.

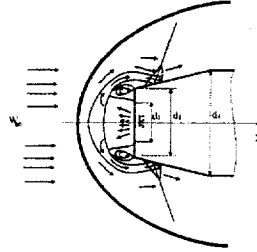


Figure 5. Schematic of the flow structure of the SPM [23]

Another important point about the flow structure of the freestream-counterflow jet interaction appears to be that it seems highly time dependent, particularly as driven by changes in the injector nozzle stagnation conditions. Thus, though the results reported here are steady state solutions, it is not clear whether the flowfield, in reality, reaches steady state, even in an asymptotical sense. Such a transient character may explain the oscillatory nature of the jets that has been observed by Formin et. al. [23] and Shang [24]. Figure 6 shows a snap shot of the solution before it converged to steady state. It is noteworthy, as we see from the figure, that the counterflow jet begins to bifurcate under the effect of the imposed momentum of the external flow with the generation of pairs of counterrotating vortices that are symmetrical about the jet axis. It is not clear whether the “states” of Fig. 4 and Fig. 6 repeat through the transient process as it goes through the SPM and the LPM as has been suggested [23].



Figure 6. A snap shot of the velocity field in time.

The above qualitative flow structure for the SPM of the counterflow jet is seen to be very well captured by the numerical prediction. Figures 7 and 8 show the quantitative comparison of the laminar flow solutions with the experimental data of Formin, et. al. [23] for the cases with and without the jet, respectively, for

normalized pressure distribution along a ray of the cone-cylinder. As can be seen from Fig. 7, the comparison shows very good agreement between the prediction and the experiment data, except close to the expansion corner where there is a paucity of data since the model appears not to have been well instrumented there. Nonetheless, the good agreement between the solution and the data for the case without the counterflow jet establishes the required confidence, as a benchmark, for the solutions for the case with the jet.

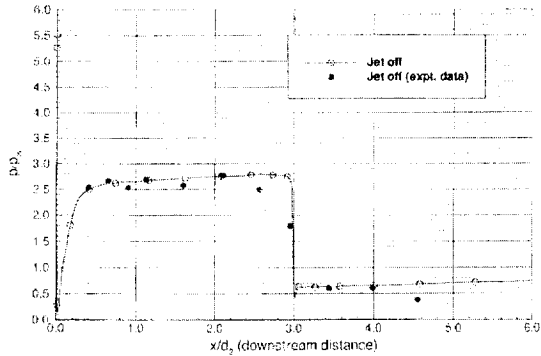


Figure 7. Variation of the normalized pressure with distance for the case without counterflow jet.

The comparison for the case with the counterflow jet is shown in Fig. 8. As one can readily see from the figure, the agreement in the surface pressure distributions is poor upstream of the expansion corner, after which the solution and the data show better agreement. However, in terms of trends, the predictions of the solution are consistent with the experimental data.

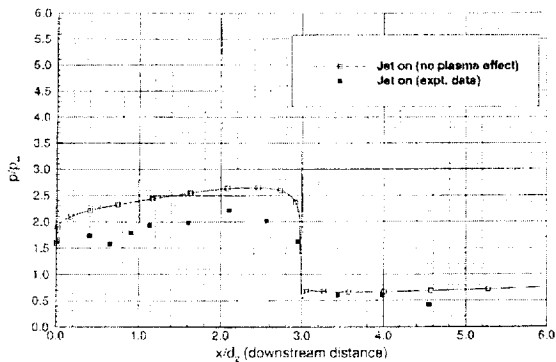


Figure 8. Variation of the normalized pressure with distance for the case with the SPM jet.

The difference between the prediction and data may be due to a variety of reasons, such as the oscillatory or transient nature of the interaction, as the jet transitions between the SPL and LPM due to instability, as discussed above. Another possibility could be the effect of the weakly ionized plasma of the counterflow jet, in

terms of additional energy release from the ionization quenching, energy transfer between the various degrees of freedom, such as vibration-translation (V-T) or vibrational relaxation, and other nonequilibrium plasma effects, in addition to Joule heating, which deposits considerable amount of energy into the flow. As stated above, we made no attempts to model such effects. Other possibilities include the effect of flow turbulence, since the boundary layer could very likely be turbulent due to the upstream interactions.

Figures 9 and 10 show the plots of the convergence rate and drag coefficient, respectively, for the case with and without the counterflow jet with solution iteration, using one level of grid sequencing. For the case without the jet, Fig. 9 shows the solution to converge to machine

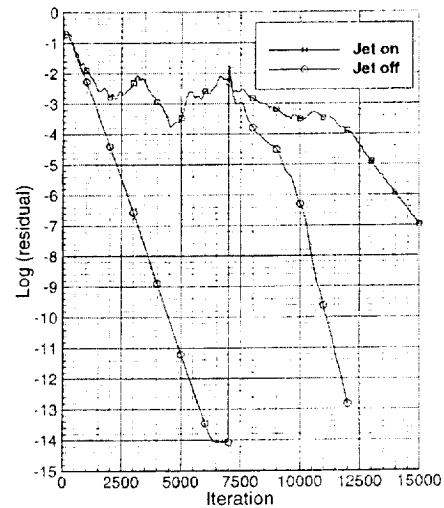


Figure 9. Residual history of truncated cone-cylinder solution with and without counterflow jet.

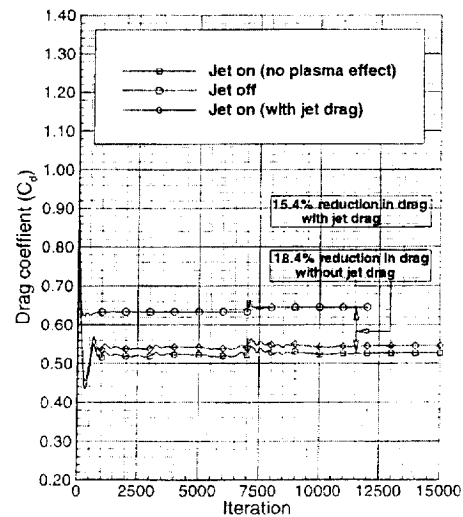


Figure 10. Variable of drag coefficient of truncated cone-cylinder solution with and without counterflow jet.

zero in terms of residual decay after about 12000 iterations. For the case with the SPM jet, the solution converged to within 7 orders of magnitude drop in residual. Even with the poor agreement in the pressure profile upstream of the expansion corner, the solution for the case with the jet shows a considerable reduction in drag, better than 18%, which reduces to about 15% when the thrust of the counterflow jet is accounted for, as Fig. 10 shows, which is exactly the same value reported by Ref. 15. A 15% reduction in drag is aerodynamically significant, particularly for transatmospheric cruise and reentry vehicles. As has been suggested, the LPM jet would give even much larger percentage in drag reduction.

Though Formin et. al. [23] stated that the counterflow jet with exit Mach number of 1 transitioned between the SPM and LPM, repeated attempts to obtain the solution for the LPM for the jet with exit Mach number of 1 was unsuccessful. Thus, to be able to calculate the flowfield for the LPM, we changed the jet exit conditions using Table 1. Computations were performed for both Mach 3 and Mach 4 counterflow jet exit conditions. We report only the Mach 3 solution here, since the Mach 4 solution was not completed because the resulting LPM jet completely penetrated or tore through the upstream computational boundary.

The solution for the jet exit Mach number of 3 is shown in Fig. 11, which shows the LPM for the Mach number distribution. It is seen that in the LPM mode, the jet penetrates upstream almost as a fluid spike or a "pencil" of fluid penetrating much further into the oncoming external freestream. The shock standoff distance is

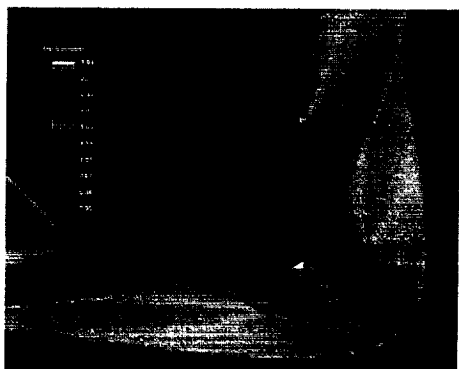


Figure 11. Mach number distribution for the LPM jet.

close to an order of magnitude larger than that of the SPM, and by implication, resulting into a significantly weaker bow shock, and therefore a much greater reduction in wave drag. Figures 12 and 13 show the solid color and contour plots of the pressure field, respectively. Also shown in Fig. 13 is the schematic of

the flow structure as given by Formin et. al. [23]. Comparison of the solution with the schematic in Fig. 13, shows a striking qualitative agreement in terms of the structure of the LPM, and, therefore, the attendant reduction of wave drag and heat flux, and any potential impact on sonic boom mitigation in terms of the strength of the ground reflected shocks [34].

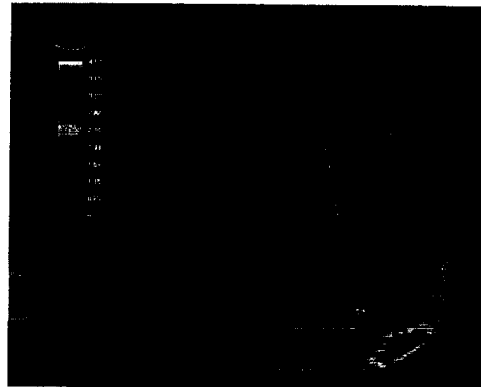
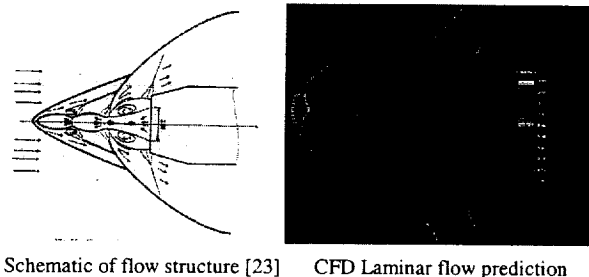


Figure 12. Pressure distribution for the LPM jet.



Schematic of flow structure [23] CFD Laminar flow prediction

Figure 13. Pressure distribution for the LPM

The penetration of the LPM can be deduced from Table 1. Table 1 shows that at $M_2 = 3$, $q_2/q_1 \cong 8.32$ and at $M_2 = 4$, $q_2/q_1 \cong 22.92$. That is the dynamic pressure of the counterflow jet with exit Mach number of 3 is more than 8 times that of the jet with exit Mach number of 1, while it is nearly 23 times larger for the jet with exit Mach number of 4. Thus, the much higher dynamic pressures provide the "punching power" of the counterflow jet to further penetrate the oncoming freestream and weaken the bow shock.

Conclusions

CFD solutions of the flowfield of a truncated cone-cylinder with and without counterflow jets have been obtained for the short and long penetration modes of the freestream-counterflow jet interaction flowfield. For the case without the counterflow jet, the comparison of the normalized surface pressures shows very good

agreement with experimental data. In the case with the counterflow SPM jet, the predicted surface pressures did not compare well with the experimental data upstream of the expansion corner, while better agreement is seen aft of the expansion corner. The disagreement between the prediction and the data could be due to the transient character of the jet penetration modes, possible effects of the plasma physics that are not accounted for here, or even the less likely effect of flow turbulence, etc.

For the LPM jet solutions, it was necessary to first use one-dimensional isentropic relations to derive the jet stagnation and exit conditions to obtain the LPM flowfield solutions. The solution for the jet exit Mach number of 3 shows a jet penetration several times longer than that of the SPM, thus, giving much weaker bow shock, with an attendant reduction in wave drag due to the much higher dynamic pressure of the jets. The LPM mode is, in essence, a "pencil" of fluid embedded in the oncoming supersonic or hypersonic freestream.

The methodology for determining the conditions for the LPM jet could enable a practical approach for the design and application of counterflow LPM jets to significantly reduce wave drag and heat flux to enhance the aerodynamic characteristics and aerothermal performance of supersonic and hypersonic vehicles. The solution shows that the qualitative flow structure is very well captured. The obtained results, therefore, suggest that counterflowing jets can be viable candidate technology concepts to significantly reduce wave drag and heat flux, in addition to other attendant aerodynamic benefits, such as sonic boom mitigation, improved lift/drag, and range by weakening the shock system about supersonic and hypersonic vehicles, such as reusable launch vehicles.

Acknowledgement

The first author wishes to thank Dr. Suk C. Kim for his many helpful comments and suggestions.

References

1. Ehrich, F., "Penetration and Deflection of Jets Oblique to a General Stream," *Journal of the Aeronautical Sciences*, Feb. 1953, pp. 99-104.
2. Resler Jr., E.L. and Sears, W.R., "The Prospects for Magneto-Aerodynamics," *Journal of the Aeronautical Sciences*, Vol. 25, April 1958, pp. 235-245.
3. Bleiviss, Z.O., "Magnetogasdynamics of Hypersonic Couette Flow," *Journal of the Aero/Space Sciences*, Vol. 25, No. 10, Oct. 1958, pp. 601-616.
4. Ziemer, R.W., "Experimental Investigation of Magnetoaerodynamics," *American Rocket Society Journal*, Vol. 19, Sept. 1959, pp. 642-646.
5. Barber, E.A., "Experimental Investigation of Stagnation Point Injection," *Journal of Spacecraft and Rockets*, Vol. 2, No. 5, 1965, pp. 770-774.
6. Romeo, D.J. and Sterret, J.R., "Flowfield for Sonic Jet Exhausting Counter to Hypersonic Mainstream," *AIAA Journal*, Vol. 3, No. 3, 1965, pp. 544-546.
7. Finley, P.J., "The Flow of a Jet from a Body Opposing a Supersonic Free Stream," *Journal of Fluid Mechanics*, Vol. 26, Part 2, 1966, pp. 337-368.
8. Workshop on Weakly Ionized Gases Proceedings, Vols. 1 and 2, USAF Academy, Colorado, June 9-13, 1997.
9. Mishin, G.I. "Experimental Investigation of the Flight of a Sphere in Weakly Ionized Air," *AIAA 97-2298*, June 1997.
10. Ghaniev, Yu.CH., Gordeev, V.P., Krasilnikov, A.V., Lagutin, V.I. and Otmennikov, V.N., "Experimental Study of the Possibility of Reducing Aerodynamic Drag by Employing Plasma Injection," 3rd International Congress on Experimental Fluid Mechanics, Kaliningrad, Moscow Region, Russia, June 3-6, 1997.
11. 2nd Weakly Ionized Gases Workshop Proceedings, Norfolk, VA, April 24-25, 1998.
12. 3rd Weakly Ionized Gases Workshop, Co-located with the 9th International Space Planes and Hypersonic Systems and Technologies Conference, Norfolk, VA, Nov. 1-5, 1999.
13. Ghaniev, Yu.CH., Gordeev, V.P., Krasilnikov, A.V., Lagutin, V.I., Otmennikov, V.N. and Panasenko, A. V., "Theoretical and Experimental Study of the Possibility of Reducing Aerodynamic Drag by Employing Plasma Injection," *AIAA 99-0603*, 1999.
14. Klimov, A., Leonov, S., Pashina, A., Skvortov, V., Cain, T. and Timofeev, B., "Influence of a Corona

- Discharge on the Supersonic Drag of an Axisymmetric Body," AIAA 99-4856, Nov. 1999.
15. Chernyi, G.G., "Some Recent Results in Aerodynamic Applications of Flow with Localized Heat Addition," AIAA 99-4819, Nov. 1999.
 16. Ganguly B. N., Bletzinger P., and Garscadden, A., "Shock Wave Damping and Dispersion In Nonequilibrium Low Pressure Argon Plasmas," *Physics Letters A*, Vol. 230, pp. 218-222, 1997.
 17. Lowry, H., Stepanek, C., Crosswy, L., Sherrouse, P., Smith, M., Price, L., Ruyten, W., and Felderman, J., "Shock Structure of a Spherical Projective in Weakly Ionized Air," AIAA 99-0600, Jan. 1999.
 18. Lowry, H., Smith, M., Sherrouse, P., Felderman, J., Drakes, J., Bauer, M., Pruitt, D., and Keefer, D., "Ballistic Range Tests in Weakly Ionized Argon," AIAA 99-4822, Nov. 1999.
 19. Van Wie, D. M., Wesner, A. L., Gauthier, L. R., "Shock Wave Characteristics Measured in Gas Discharges," 3rd AIAA Weakly Ionized Gases Workshop, AIAA 99-4824, Nov. 1999.
 20. Kunhardt, E., Saeks, R., Mankowski, J. and Suchomel, C., "One Dimensional Shock Characteristics in Weakly Ionized Gases," AIAA 99-4941, Nov. 1999.
 21. Beaulieu, W., Bytyurin, V., Klimov A., et. al., "Plasma Aerodynamic Wind Tunnel Tests With 1/6 Scale Model of Nose Part of F-15," AIAA 99-4825, Nov. 1999.
 22. Malmuth, N.D., Formin, V.M., Maslov, A.A., Fomichev, V.P. Shashkin, A.P., Korotaeva, T.A., Shipliyuk, A.N. and Pozdnyakov, G.A., "Influence of Counterflow Jet on Supersonic Blunt-Body Pressures," AIAA 99-4883, Nov 1999.
 23. Formin, V.M., Maslov, A.A., Malmuth, N.D., Fomichev, V.P. Shashkin, A.P., Korotaeva, T.A., Shipliyuk, A.N. and Pozdnyakov, G.A., "Influence of Counterflow Jet on Supersonic Blunt-Body Pressures," *AIAA Journal.*, Vol. 40, No. 6, June 2002, pp. 1170-1177.
 24. Shang, J.S., "Plasma Injection for Hypersonic Blunt-Body Drag Reduction," *AIAA Journal.*, Vol. 40, No. 6, June 2002, pp. 1178-1186.
 25. Macheret, S.O., Martinelli, L., and Miles, R.B., "Shock Wave Propagation and Structure in Non-Uniform Gases and Plasmas," AIAA 99-0598, Jan. 1999.
 26. Macheret, S.O., Ionikh, Y.Z., Martinelli, L., Barker, P.F. and Miles, R.B., "External Control of Plasmas for High-Speed Aerodynamics," AIAA 99-4853, Nov. 1999.
 27. White, A.R., Essenhigh, K.A., Adamovich, I., Lempert, W. and Subramaniam, V.V. AIAA 99-4855, Nov. 1999.
 28. Riggins, D.W., Nelson, H.F. and Johnson, E., "Blunt Body Wave Drag Reduction Using Focused Energy Deposition," AIAA 98-1647, April 1998.
 29. Riggins, D.W. and Nelson, H.F., "Hypersonic Flow Control Using Upstream Focused Energy Deposition," AIAA 98-0898, Jan. 1999.
 30. Nelson, H.F., Meyer, B and Riggins, D.W., "Supersonic Drag and Heat Transfer Reduction Using a Forward," AIAA 4880, Nov. 1999.
 31. Poggie, J., "Modeling the Effects of Weak Ionization on Supersonic Flow and Shock Waves," AIAA 99-0867, Jan. 1999.
 32. Candler, G.V., and Kelley, J.D., "Effect of Internal Energy Excitation on Supersonics Blunt Body Drag," AIAA 99-0418, Jan. 1999.
 33. Candler, G.V., and Kelley, J.D., "Effect of Internal Energy Excitation on Supersonics Air Flow," AIAA 99-4964, Nov. 1999.
 34. Marconi, F., "An Investigation of Tailored Upstream Heating for Sonic Boom and Drag Reduction," AIAA 98-0333, Jan. 1998.
 35. Krist, S.L., Biedron, R.T. and Rumsey, C.L., "CFL3D User's Manual, Ver. 5.0," NASA Langley, Research Center, Sept. 1997.